

# Dual-Rotor Luminescence Based on Supramolecular Secondary Reassembly

Wen-Wen Xu, Yue-Xiu Qin, Jie Niu, Wenshi Xu, Yong Chen, Heng-Yi Zhang, and Yu Liu\*

Herein, synergistically confining anthracene-phenylpyridium derivatives (**1'** and **1**) as dual-rotor luminogens through macrocyclic cucurbit[8]uril (CB[8]) and hyaluronic acid (HA) mediated supramolecular secondary reassembly is reported to give bright fluorescence emission. The non-emissive dual-rotor molecule **1** first assembles with CB[8] to form non-emissive supramolecular nanotubes, which are further reconstructed to be nanoparticles with a diameter of 83 nm by HA induced secondary reassembly through electrostatic interaction. Intriguingly, the secondary reassembly not only transforms the topological morphology, but also acts as a switch to activate the robust fluorescence of dual-rotor molecule, accompanying emission at 600 nm with large Stokes shift (150 nm). This activation is mainly attributed to sufficient suppression of intramolecular rotation and promotion of intramolecular charge transfer of dual-rotor molecule after reassembly. Benefiting from multiple components synergistic stimuli-responsiveness and the targeted ability of HA to tumor cells, the secondary reassembly constructed dual-rotor luminescence system is successfully applied in triplet encryption information security and targeted cancer cell imaging.

exploration of new chromophores and stimuli-responsive luminogens, and so on.<sup>[7]</sup> As efficient means and strategies, supramolecular assembly and host-guest chemistry exhibit numerous advantage in facilitating fluorescence emission of organic small molecules.<sup>[8]</sup> Particularly, macrocyclic compounds with unique cavity structure, such as cyclodextrins,<sup>[9]</sup> cucurbiturils,<sup>[10]</sup> crown ethers,<sup>[11]</sup> and so on,<sup>[12]</sup> can form host-guest complexes or supramolecular assemblies with organic molecules to keep from quenching caused by molecular motion or aggregation, and have been widely used to construct smart luminescent materials.

Intriguingly, benefiting from the photo-responsive characteristic of smart materials, more and more luminescent technologies have been developed to construct security systems for protecting confidential information and bioimaging agents for disease diagnosis and surgical navigation.<sup>[13]</sup> For instance,

Zhang and co-workers reported the printable off-on thermostwitchable fluorescence materials for multiple encryption through a thermally induced synchronous “dual-multichannel” stimulus-response mode.<sup>[13a]</sup> Ameloot and coworkers illustrated anthracene-loaded metal organic frameworks to perform encryption and decryption of information through the photoresponse of photodimerization of anthracene.<sup>[13e]</sup> In addition, Rosenthal's group developed an approach for determining tumor margins with surgical specimen mapping through use of near-infrared fluorescence.<sup>[13i]</sup> Recently, Yu and co-workers designed a NIR-II emissive dye SQ890 based on polymer nanoparticle for targeting photothermal therapy of oral cancer.<sup>[13j]</sup> Although there are some luminescent researches for information encryption and cancer diagnosis and surgical navigation, with the development of modern technology, more advanced luminescent technology by integrating multiple functions in one system is of urgency to be explored.

Herein, two anthracene-centered chromophores, 4,4'-(anthracene-9,10-diylbis(4,1-phenylene)) bis(1-methylpyridin-1-ium) chloride (**1**) and 4-(4-(anthracen-9-yl)phenyl)-1-methylpyridin-1-ium chloride (**1'**) with dual-rotor properties were reported to achieve bright fluorescence with large Stokes shift synergistically activated by cucurbit[8]uril (CB[8])/HA mediated supramolecular secondary reassembly (**Figure 1**). Firstly, the molecules **1** and **1'** were non-emissive under single molecular state and emitted robust fluorescence under aggregated state, suggesting the obvious AIE performance. Intriguingly, after complexing with CB[8] through ion-dipole interaction, the non-emissive molecules **1** and **1'** respectively formed non-emissive

## 1. Introduction

The 2008 and 2014 Nobel Prizes in Chemistry were awarded to the scientists working on the researches of green fluorescent protein and supra-resolution fluorescent microscopy, respectively, which greatly manifests the significance and importance of luminescent technique in our daily life. Comparing to inorganic materials, organic luminescent materials due to their readily access, diverse functionalization, rich source, and excellent biocompatibility have attracted widespread interest and are applied in fields of bioimaging,<sup>[1]</sup> sensing devices,<sup>[2]</sup> detection,<sup>[3]</sup> photoelectric devices,<sup>[4]</sup> anti-counterfeiting,<sup>[5]</sup> and so on.<sup>[6]</sup> Over the past several decades, massive efforts have been made to obtain high-performance organic fluorescent materials, including design of delayed fluorescence,

W.-W. Xu, Y.-X. Qin, J. Niu, W. Xu, Y. Chen, H.-Y. Zhang, Y. Liu  
 Department of Chemistry  
 State Key Laboratory of Elemento-Organic Chemistry  
 Nankai University  
 Tianjin 300071, P. R. China  
 E-mail: yuliu@nankai.edu.cn

Y. Liu  
 Collaborative Innovation Center of Chemical Science and Engineering  
 Tianjin 300071, P. R. China

 The ORCID identification number(s) for the author(s) of this article can be found under <https://doi.org/10.1002/adom.202202431>.

DOI: 10.1002/adom.202202431

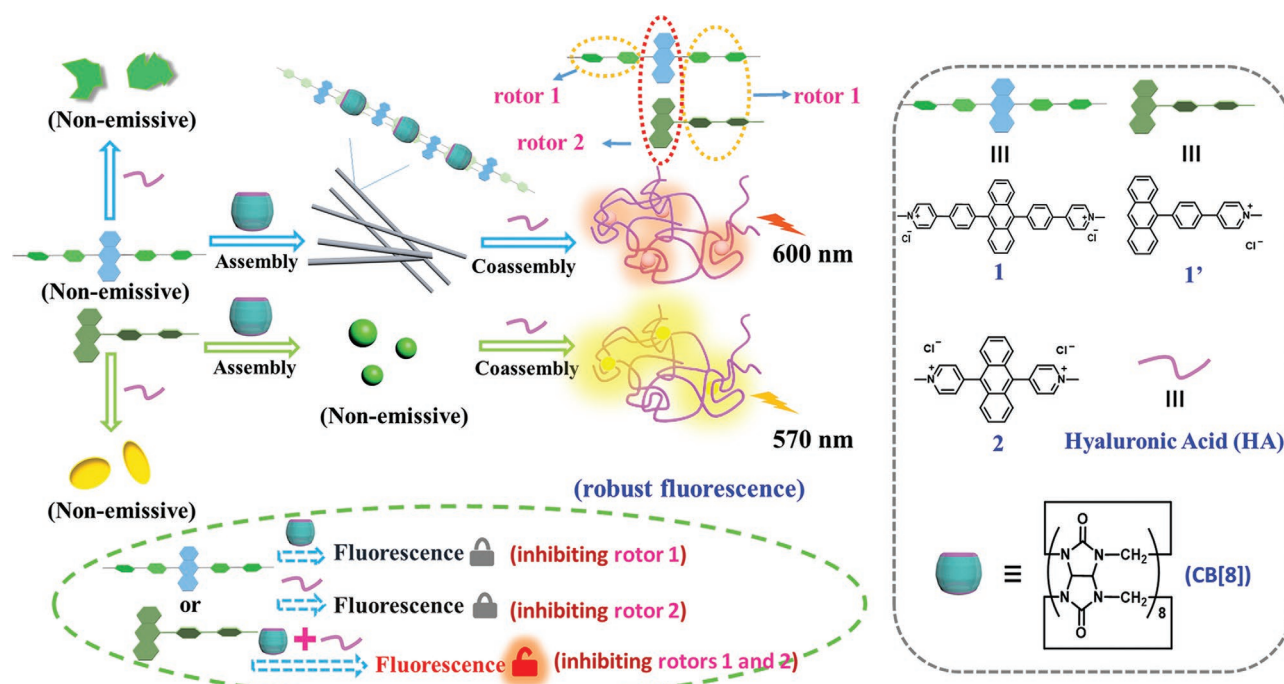


**Figure 1.** The schematic illustration of dual-rotor luminescence activated by supramolecular secondary reassembly.

supramolecular nanotubes and nanoparticles, which were further reconstructed to be smaller nanoparticles by HA through electrostatic interaction. The reconstructed nanoparticles were able to exhibit robust fluorescence emission at 570 nm (1') and 600 nm (1). Different from the aggregated state in solid (4.47% for 1 and 9.95% for 1'), the quantum yield results showed that the fluorescence induced by supramolecular secondary reassembly (10.01% for 1 and 66.83% for 1') presented higher luminescence efficiency, proving the outstanding effect of supramolecular assembly on inducing luminescence behavior of organic small molecules. The mechanism researches revealed that the fluorescence performance mainly originated from two factors: 1) CB[8] and HA precisely suppressing the intramolecular rotation of phenylpyridinium (rotor 1) and anthracene (rotor 2), respectively; 2) formation of charge transfer from anthracene to phenylpyridinium. Hence, CB[8] and HA as two crucial keys to unlock the fluorescence emission were interdependent in the luminescent systems. Combining with the targeted ability of HA and dual-rotor luminescent traits, the secondary reconstructed nanoparticles are successfully applied in targeted bioimaging for cancer cells and triplet encryption information security, hinting the huge potential application in biomaterials and multilevel stimuli-responsive smart luminescent materials.

## 2. Results and Discussion

### 2.1. Structural Characteristics and Photophysical Properties

Firstly, three anthracene-centered emitters (1, 1', and 2) were synthesized by Suzuki coupling reaction, nucleophilic substitution, and ion exchange procedures in sequence (Schemes S1–S3, Supporting Information). Compound 2 was prepared to explore

the effect of phenyl between anthracene and pyridinium on the photophysical performance of anthracene-centered emitters. The  $^1\text{H}$  and  $^{13}\text{C}$  nuclear magnetic resonance (NMR) experiments and high resolution mass spectrum (HRMS) were used to characterize and prove the structures of compounds 1, 1', and 2 (Figures S1–S15, Supporting Information). In addition, the UV–vis absorption spectrum, fluorescence spectrum, and time-resolved photoluminescence decay plot were utilized to record the photophysical properties of compounds 1, 1', and 2 in solid and in aqueous. The topological morphologies of supramolecular assembly were tested by transmission electron microscope (TEM). The dynamic light scattering (DLS) and zeta potential ( $\zeta$ ) were used to afford the size distribution and to estimate the charge and potential of supramolecular assembly, respectively.

As revealed by the UV–vis absorption spectra, there were three characteristic absorption bands for compounds 1 (250, 292, and 392 nm) and 1' (250, 295, and 383 nm), respectively (Figure S16a, Supporting Information). Although there was a subtle difference in absorption wavelength, three similar characteristic absorption peaks for compounds 1 and 1' suggested that the amount of phenylpyridinium conjugated to anthracene had little effect on the absorption band of this class of molecules. Nevertheless, the lack of phenyl between anthracene and pyridinium caused that the compound 2 only exhibited two characteristic absorption bands, located at 250 and 398 nm, respectively. In order to classify different ultraviolet absorption bands of molecule 1 and 1', the reference molecules 2-anthracic acid and 1-methyl-4-phenylpyridinium chloride were selected (Scheme S4, Supporting Information). The UV–vis spectra showed that molecule 2-anthracic acid presented narrow absorption peak at around 250 nm and broad peak at 300–400 nm, respectively (Figure S16b, Supporting Information). Another

molecule 1-methyl-4-phenylpyridin-1-ium chloride only presented one absorption peak at around 290 nm. Thereby, it was rational to deduce that the three absorption bands of molecules 1 and 1' belonged to the characteristic absorption of anthracene (around at 250 and 390 nm) and phenylpyridinium (around at 290 nm), respectively. In other words, there was nonconjugated structure between anthracene and phenylpyridinium for molecules 1 and 1'. Afterward, the photophysical performance of compounds was further studied. Considering the possible interference of artifactual peaks from light source in emission spectra when excited by short wavelength light sources, the reddest absorption bands were chosen as excitation wavelengths. Intriguingly, the fluorescence spectra and photographs showed that there was no any emission for compounds 1 and 1' in aqueous (Figure S16c, Supporting Information). On the contrary, the compound 2 emitted strong yellow fluorescence at 542 nm with lifetime of 1.99 ns (Figures S16c and S17, Supporting Information). The distinct photophysical properties hinted that the phenyl between anthracene and pyridinium had a great influence on the luminescent behavior of this class of anthracene-centered emitters. We speculated that the compounds 1 and 1' could dissipate the energy of excited state through intramolecular rotation due to large steric hindrance between phenylpyridinium and anthracene, similar to AIE molecule tetraphenylethene.<sup>[8h]</sup> Nevertheless, the lack of phenyl

promoted the compound 2 to form charge transfer stable state from anthracene to pyridinium to reduce intramolecular rotation, thus resulting in the fluorescence of compound 2. Therefore, the phenyl between anthracene and pyridinium might act as a switch for tuning the luminescent properties of these anthracene-centered emitters.

To further probe the difference of photophysical performance, the experiments of introducing poor solvents to the solutions of 1, 1', and 2 were performed to detect the emissive properties under aggregated state. As shown in the fluorescence spectra, when gradually increasing the ratio of poor solvents to change the chromophores from single molecular state to aggregated state, compounds 1 and 1' successfully transformed from non-emissive state to bright emissive state, with emission wavelengths at 600 and 576 nm, respectively (Figure 2a,b,d,e). This change indicated that forming aggregated state benefited for generating fluorescence, further confirming the AIE properties of compounds 1 and 1'. As a contrast, the fluorescence of molecule 2 only presented enhancement when introducing poor solvent (Figure S18, Supporting Information). Additionally, the solid luminescence was also investigated. According to the spectral analysis and photographs, all anthracene-centered chromophores exhibited bright fluorescence emission in solid state. Compounds 1 and 1' emitted red fluorescence at 625 nm with maximum excitation wavelength at 467 nm and yellow

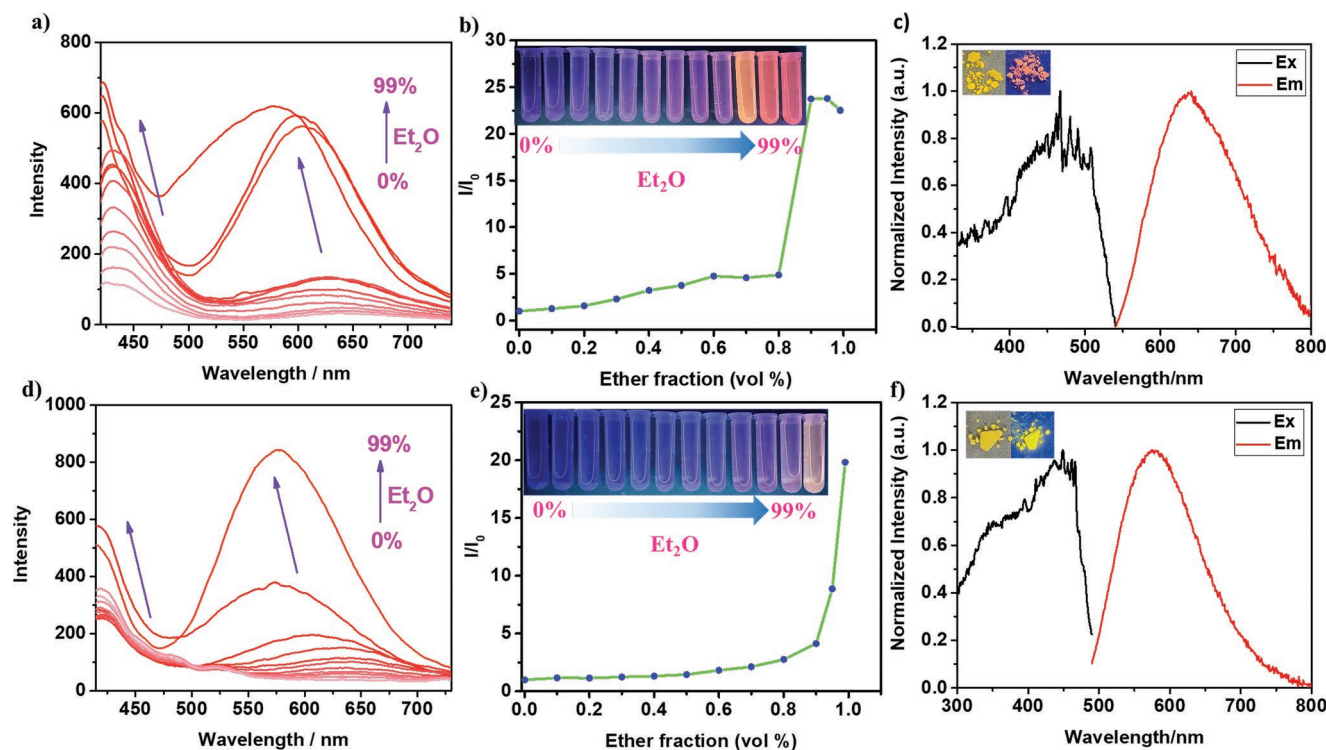


**Figure 2.** a) Fluorescence spectra of 1 ( $[1] = 1 \times 10^{-5}$  M) in mixed solvents MeOH/Et<sub>2</sub>O with gradually increasing the ratio of poor solvent (Et<sub>2</sub>O); b) The intensity ratio of  $I$  and  $I_0$ ,  $I$  represents the fluorescence intensity of 1 at 600 nm in mixed solvents and  $I_0$  represents the original fluorescence intensity of 1 in MeOH (inset: the photographs of 1 in mixed solvents MeOH/Et<sub>2</sub>O with increasing the ratio of Et<sub>2</sub>O under irradiation of 365 nm UV light); c) The excitation (black) and emission (red) spectra of molecule 1 in solid state (inset: photographs under daylight (left) and 365 nm UV light (right)); d) Fluorescence spectra of 1' ( $[1'] = 1 \times 10^{-5}$  M) in mixed solvents MeOH/Et<sub>2</sub>O with gradually increasing the ratio of poor solvent (Et<sub>2</sub>O); e) The intensity ratio of  $I$  and  $I_0$ ,  $I$  represents the fluorescence intensity of 1' at 576 nm in mixed solvents and  $I_0$  represents the original fluorescence intensity of 1' in MeOH solution (inset: the photographs of 1' in mixed solvents MeOH/Et<sub>2</sub>O with increasing the ratio of Et<sub>2</sub>O under irradiation of 365 nm UV light); f) The excitation (black) and emission (red) spectra of molecule 1' in solid state (inset: photographs under daylight (left) and 365 nm UV light (right)).

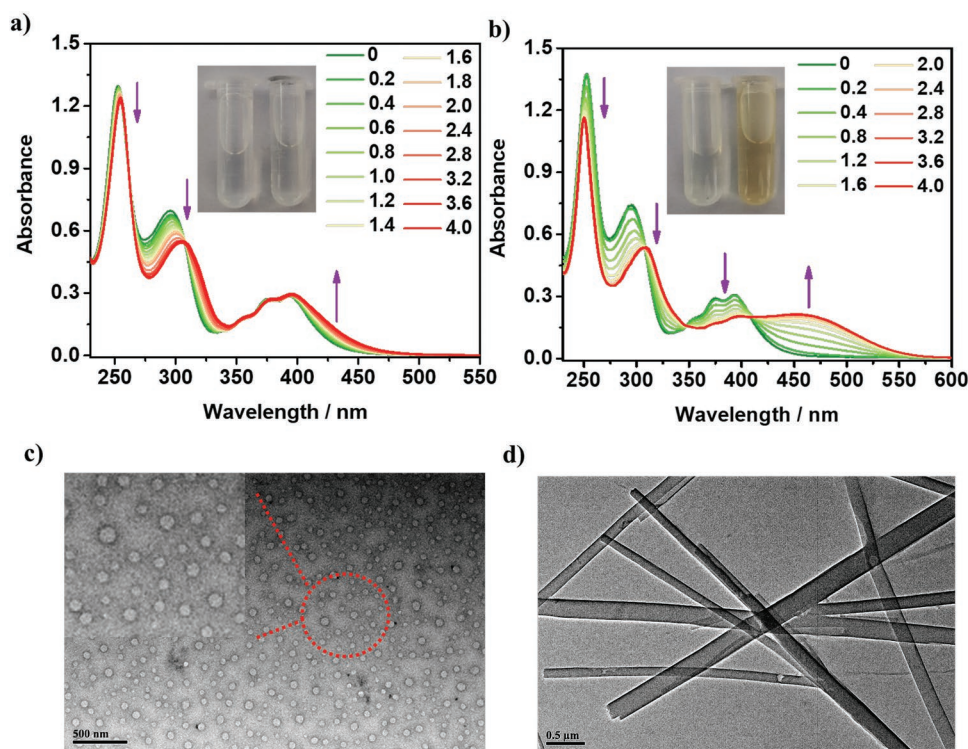


**Figure 3.** UV-vis absorption spectra of 1 ( $[1] = 2 \times 10^{-5} \text{ mol L}^{-1}$ ) with different concentrations of a) CB[7] (from 0 to 4 eq.) and b) CB[8] (from 0 to 4 eq.) in aqueous at 25 °C (inset: the photographs of 1 in aqueous before (left) and after (right) adding CB[7] or CB[8] under daylight); The TEM images of host-guest complexes c) 1/CB[7] and d) 1/CB[8].

fluorescence at 566 nm with maximum excitation wavelength at 450 nm, respectively, and the compound 2 presented cyan fluorescence at 490 nm with maximum excitation wavelength at 440 nm (Figure 2c,f and Figure S19, Supporting Information). The time-resolved photoluminescence decay spectra depicted that the fluorescence lifetimes were 4.53 nanoseconds (ns) for compounds 1, 8.01 ns for compound 1', and 7.05 ns for compound 2, respectively (Figure S20, Supporting Information). The quantum yield results showed that the luminescence efficiency was 4.47% (1), 9.95% (1'), and 40.38% (2), respectively (Figures S21–S23, Table S1, Supporting Information). These results were greatly consistent with the aforementioned conclusion and effectively proved the AIE behavior of compounds 1 and 1', that was to say, the compounds 1 and 1' could exhaust the energy through intramolecular rotation under single molecular state. But which part of anthracene or phenylpyridinium dissipated the energy of the excited state, or did both work? Is there any other measure to restrict this intramolecular rotation beside adding organic poor solvents? It is of great urgency for us to find these answers.

For this purpose, the strategies of host-guest chemistry and supramolecular assembly, known as effective measures to induce or enhance luminescent behavior of organic small molecules,<sup>[8a,b,10]</sup> were introduced to improve the photophysical behavior of compounds 1 and 1'. As reported in previous works, our team realized excellent phosphorescence emission of phenylpyridinium derivatives by complexing with macrocyclic host cucurbiturils, implying the excellent efficiency of

supramolecular strategies.<sup>[14]</sup> Furthermore, the moiety of pyridinium is known as guest able to complex with cucurbit[n]uril ( $n = 7, 8$ ) to form corresponding host-guest complexes. In order to fully observe the behavior of host-guest complexation and change of photophysical properties, various molar ratios of CB[ $n$ ] ( $n = 7, 8$ ) were used to complex with molecules 1 and 1' and to study the trend of change. The UV-vis absorption spectra showed that the corresponding characteristic absorption of compounds 1 and 1' decreased obviously and eventually maintained constant as gradually increasing the ratio of CB[7] (Figure 3a and Figure S24a, Supporting Information). Compared to CB[7], the complexation of CB[8] not only reduced the characteristic absorption of compounds 1 and 1', but also induced the new absorption band at 450 and 424 nm, which was attributed to the charge transfer from anthracene to pyridinium due to the formation of host-guest complex between guests (1 or 1') and CB[8] (Figure 3b and Figure S24b, Supporting Information). However, there was no change and occurrence of new absorption band for host-guest complex from reference molecule (1-methyl-4-phenylpyridin-1-ium chloride) and CB[8], proving that the

## 2.2. Host-Guest Complexes

Hence, these anthracene-centered emitters were separately utilized as guests to complex with cucurbit[ $n$ ]uril ( $n = 7, 8$ ) to form corresponding host-guest complexes. In order to fully observe the behavior of host-guest complexation and change of photophysical properties, various molar ratios of CB[ $n$ ] ( $n = 7, 8$ ) were used to complex with molecules 1 and 1' and to study the trend of change. The UV-vis absorption spectra showed that the corresponding characteristic absorption of compounds 1 and 1' decreased obviously and eventually maintained constant as gradually increasing the ratio of CB[7] (Figure 3a and Figure S24a, Supporting Information). Compared to CB[7], the complexation of CB[8] not only reduced the characteristic absorption of compounds 1 and 1', but also induced the new absorption band at 450 and 424 nm, which was attributed to the charge transfer from anthracene to pyridinium due to the formation of host-guest complex between guests (1 or 1') and CB[8] (Figure 3b and Figure S24b, Supporting Information). However, there was no change and occurrence of new absorption band for host-guest complex from reference molecule (1-methyl-4-phenylpyridin-1-ium chloride) and CB[8], proving that the

charge transfer was not due to the dimerization of phenylpyridinium in cavity of CB[8] (Figure S25, Supporting Information). In addition, the appearance of 1 and 1' changed from colorless to orange after adding CB[8], further proving the variety of absorption band. Moreover, <sup>1</sup>H NMR experiments validated that chemical shift of the moiety of phenylpyridinium obviously shifted and were broadened when adding CB[7] or CB[8] (Figures S26 and S27, Supporting Information). For the complexes constructed by 1 and CB[8], particularly, all characteristic peaks of 1 were broadened, indicating that 1 might form linear supramolecular polymer with CB[8] via *n* (host):*n* (guest) binding mode, but not 2:2 host–guest complex.<sup>[10c,d]</sup> The Job's plot confirmed that the binding ratios were 1 (guest):2 (host) for compound 1 and CB[7], 1 (guest):1 (host) for compound 1' and CB[7], 1 (guest):1 (host) for compound 1 and CB[8], 2 (guest):1 (host) for compound 1' and CB[8], respectively (Figures S28 and S29, Supporting Information). Additionally, the TEM images showed that the topological morphology of 1 and 1' changed from nanoparticles to vesicles after complexing with CB[7], and 1' maintained the unchanged morphology of nanoparticle after complexing with CB[8] (Figure 3c, Figures S30 and S31, Supporting Information). Nevertheless, 1/CB[8] presented the morphology of nanotube, which strongly manifested the assumption of linear supramolecular polymer fabricated by 1 and CB[8] (Figure 3d). These results jointly demonstrated that the compounds 1 and 1' were appropriate guests to complex with macrocyclic compounds CB[*n*] (*n* = 7, 8) to form corresponding host–guest complexes. However, the almost unchanged UV–vis absorption spectra and unchanged appearance of solution confirmed that molecule 2 was unsuitable guest to construct host–guest inclusion with CB[*n*] (*n* = 7, 8), which was due to the large steric hindrance from anthracene causing that the moiety of pyridinium could not thread the cavity of CB[*n*] (*n* = 7, 8) (Figure S32, Supporting Information).

The spectral analysis suggested that compounds 1 and 1' were still non-emissive although complexing with CB[*n*] (*n* = 7, 8), which made us believe this assumption of dual-rotor (Figure S33, Supporting Information). Both anthracene and phenylpyridinium play the roles in depleting the energy of excited state in luminogens by means of rotation. Although the complexation of macrocyclic cucurbiturils can suppress the rotation of phenylpyridinium (rotor 1), the part of anthracene (rotor 2) is still exposed and can dissipate the energy by free rotation. To confirm the deduction, the strategy of supramolecular secondary assembly is selected to further restrain the molecular motion and rotation. Considering the positive charge of pyridinium in 1 and 1', the negatively charged polysaccharide HA is used to coassemble with the abovementioned host–guest complexes through electrostatic interaction.

### 2.3. Supramolecular Secondary Reassembly

The bright luminescence proved the efficacy of supramolecular secondary assembly. With adding HA in the host–guest complexes, the strong fluorescence emissions were activated and observed for ternary supramolecular systems 1/CB[8]+HA and 1'/CB[8]+HA. The spectral researches demonstrated the

fluorescence properties. The fluorescence spectra showed that the emissions were located at 600 nm for 1/CB[8]+HA corresponding to orange fluorescence and 570 nm for 1'/CB[8]+HA corresponding to yellow fluorescence, respectively (Figure 4a,d). The time-resolved photoluminescence decay spectra and quantum yield results showed that the lifetimes and quantum yields were 5.85 ns and 10.01% for 1/CB[8]+HA, 9.28 ns and 66.83% for 1'/CB[8]+HA, respectively, (Figure 4b,e, Figures S34 and S35, Supporting Information). Specially, the high luminescence efficiency from supramolecular secondary assembly (10.01% for 1/CB[8]+HA and 66.83% for 1'/CB[8]+HA) had exceeded that of aggregated state in solid (4.47% for 1 and 9.95% for 1'), revealing the superior effect of supramolecular assembly in inducing luminescence of organic molecules. Interestingly, it was found that the ternary supramolecular systems 1/CB[8]+HA and 1'/CB[8]+HA were able to generate the fluorescence with same emission wavelength and emission intensity under various excitation wavelengths (250, 292, and 450 nm for 1/CB[8]+HA, 250, 295, and 424 nm for 1'/CB[8]+HA), which was in agreement with the kasha's rule (Figure S36, Supporting Information). This phenomenon explained that the excited electrons returned to the ground state through the same excited energy level whatever the absorption of anthracene, phenylpyridinium or charge transfer absorption from anthracene to phenylpyridinium was chosen as excitation wavelength. With the lowest-level absorption as excitation wavelengths, the corresponding Stokes shifts were calculated as large as 150 nm for 1/CB[8]+HA and 146 nm for 1'/CB[8]+HA, respectively. When changing the order of supramolecular assembly through first mixing molecules 1 or 1' with HA and then adding CB[8], the fluorescence intensity slightly decreased (Figure S37, Supporting Information). This was probably because CB[8] was more difficult to complex with molecule 1 or 1' under polymer (HA) environment. Nevertheless, no signals were detected when host–guest complexes 1/CB[7] and 1'/CB[7] further coassembled with HA (Figure 4c,f and Figure S38, Supporting Information). Besides, the bright fluorescence of 1 and 1' could also not be activated by directly mixing compounds 1 or 1' with negatively charged polysaccharide HA. These experiments not only effectively proved the dual-rotor properties of this class of anthracene-center emitters, but also demonstrated that both CB[8] and negatively charged polysaccharide HA were two indispensable keys for unlocking the fluorescence of molecules 1 and 1'. Since compound 2 was able to emit fluorescence by itself in aqueous, the fluorescence was only enhanced (less than double), and there was no activated behavior similar to compounds 1 and 1' (Figure S39, Supporting Information). Due to change of hydrophobic microenvironment around molecule 2 after assembling with cucurbiturils or HA through ion–dipole interaction or electrostatic interaction, the emission exhibited slight hypochromatic shift. Moreover, the almost unchanged fluorescence intensity for 2/CB[8] and 2/CB[8]+HA suggested that the introduction of HA had no obvious effect on the fluorescence emission of compound 2, which was greatly distinct from the compounds 1 and 1'. The time-resolved photoluminescence decay plots presented similar lifetimes (6.40 ns for 2+CB[8] and 6.26 ns for 2+CB[8]+HA), further validating this conclusion (Figure S40 and Table S1, Supporting Information).

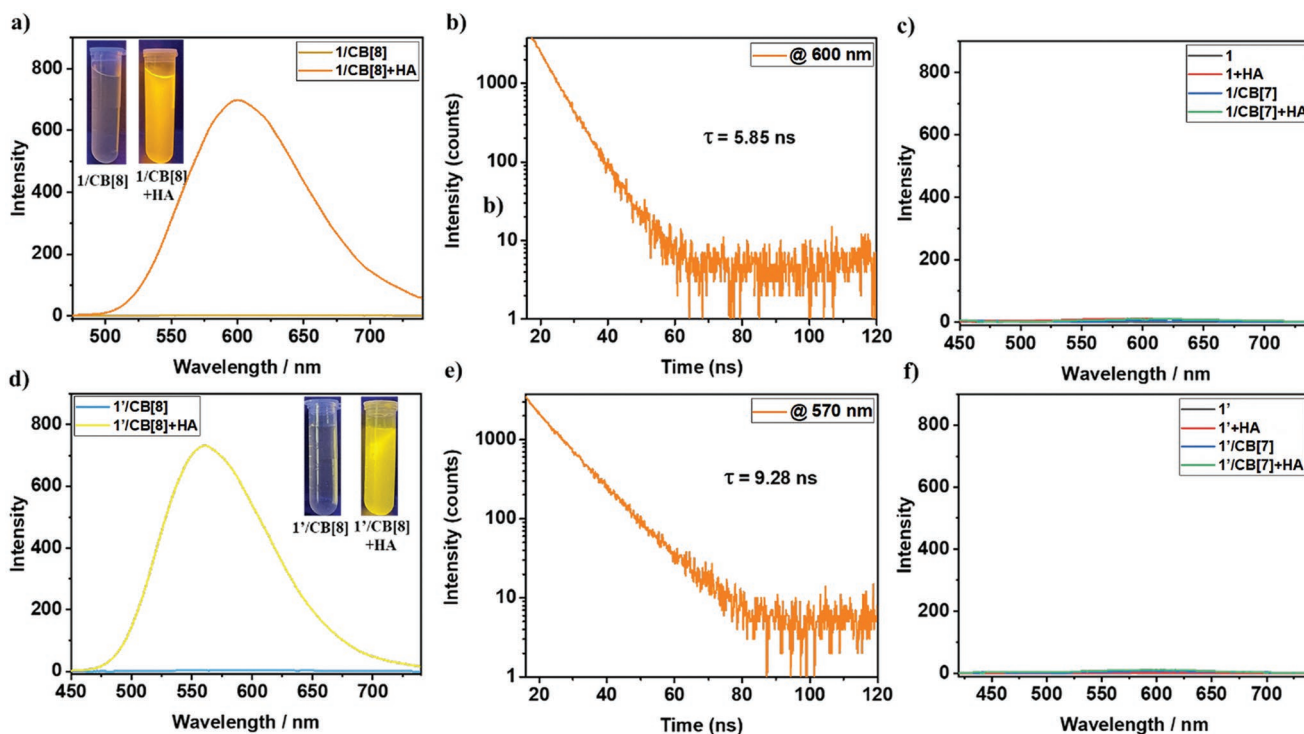


**Figure 4.** a) The fluorescence spectra of 1/CB[8] and 1/CB[8]+HA (excitation wavelength: 450 nm, excitation/emission slit: 10/2.5 nm,  $[1] = [\text{CB}[8]] = 2 \times 10^{-5}$  M,  $[\text{HA}] = 4 \times 10^{-6}$  M, inset: the photographs of 1/CB[8] before and after adding HA under irradiation of 365 nm UV light); b) The time-resolved photoluminescence decay spectrum of 1/CB[8]+HA at 600 nm in aqueous; c) The fluorescence spectra of 1, 1+HA, 1/CB[7] and 1/CB[7]+HA (excitation wavelength: 392 nm, excitation/emission slit: 10/2.5 nm,  $[1] = 2 \times 10^{-5}$  M,  $[\text{CB}[7]] = 4 \times 10^{-5}$  M,  $[\text{HA}] = 4 \times 10^{-6}$  M); d) The fluorescence spectra of 1'/CB[8], 1'/CB[8]+HA (excitation wavelength: 424 nm, excitation/emission slit: 10/2.5 nm,  $[1'] = 2 \times 10^{-5}$  M,  $[\text{CB}[8]] = 1 \times 10^{-5}$  M,  $[\text{HA}] = 4 \times 10^{-6}$  M, inset: the photographs of 1'/CB[8] before and after adding HA under irradiation of 365 nm UV light); e) The time-resolved photoluminescence decay spectrum of 1'/CB[8]+HA at 570 nm in aqueous; f) The fluorescence spectra of 1', 1'+HA, 1'/CB[7], 1'/CB[7]+HA, (excitation wavelength: 383 nm, excitation/emission slit: 10/2.5 nm,  $[1'] = [\text{CB}[7]] = 2 \times 10^{-5}$  M,  $[\text{HA}] = 4 \times 10^{-6}$  M).

## 2.4. Effects of Polysaccharide

Due to the uniqueness and superiority of supramolecular secondary assembly in inhibiting the intramolecular rotation of dual-rotor luminogens, the fluorescence of anthracene-centered emitters 1 and 1' had been successfully ignited by complexing with CB[8] based on ion-dipole interaction and further co-assembling with HA through electrostatic interaction. In the meantime, we also explored the effects of molecular weight, concentration of HA and the type of polysaccharide on the photophysical properties. With 1/CB[8] as an example, the fluorescence intensity was positively correlated with the concentration of HA (Figure S41, Supporting Information). The higher concentration of HA meant stronger fluorescence emission before the concentration of HA reached  $4 \times 10^{-6}$  M (0.2 eq. to molecule 1). Similar phenomenon was observed when we gradually increased the ratio of CB[8] with fixing concentration of molecule 1 ( $2 \times 10^{-5}$  M) and HA ( $4 \times 10^{-6}$  M) (Figure S42, Supporting Information). The fluorescence intensity presented maximum value and almost maintained unchanged as the concentration of CB[8] exceeded  $2 \times 10^{-5}$  M (1.0 eq. to molecule 1). Therefore, the optimal molar ratio to acquire the excellent luminescence efficiency was chosen as 1 (molecule 1): 0.2 (HA). Besides, HA with various molecular weights (3000, 5000, 10 000, 100 000) was used to coassemble with 1/CB[8]

to prepare a series of ternary supramolecular systems. The results showed that the fluorescence emission of ternary supramolecular system 1/CB[8]+HA almost remained unchanged when changing the molecular weight of HA, demonstrating that the molecular weight of HA would not affect the fluorescence efficiency (Figure 5b). In addition, the various types of polysaccharides, including negatively charged chondroitin sulfate (ChS), sodium alginate (SA) and positively charged chitosan (CS), were utilized to coassemble with 1/CB[8] to probe the influence of the types of polysaccharides (Figure 5a). The fluorescence spectra exhibited that both ChS and SA were capable of inducing the fluorescence emission of 1/CB[8], although the enhanced effect was not as good as HA (Figure 5c and Figure S43, Supporting Information). The lifetimes and quantum yields of corresponding fluorescence were 6.01 ns and 3.09% for 1/CB[8]+ChS, 6.15 ns and 6.15% for 1/CB[8]+SA, respectively (Figures S44–S46, Table S1, Supporting Information). Similar to HA, the fluorescence was gradually enhanced and finally reached constant when increasing the concentration of ChS and SA (Figure S47, Supporting Information). However, no fluorescence emission was captured for ternary supramolecular system based on 1/CB[8] and CS, indicating that the positively charged CS was unable to activate the fluorescence of 1/CB[8]. This was probably attributed to the positively charged species of CS. The host-guest complex 1/CB[8] showed

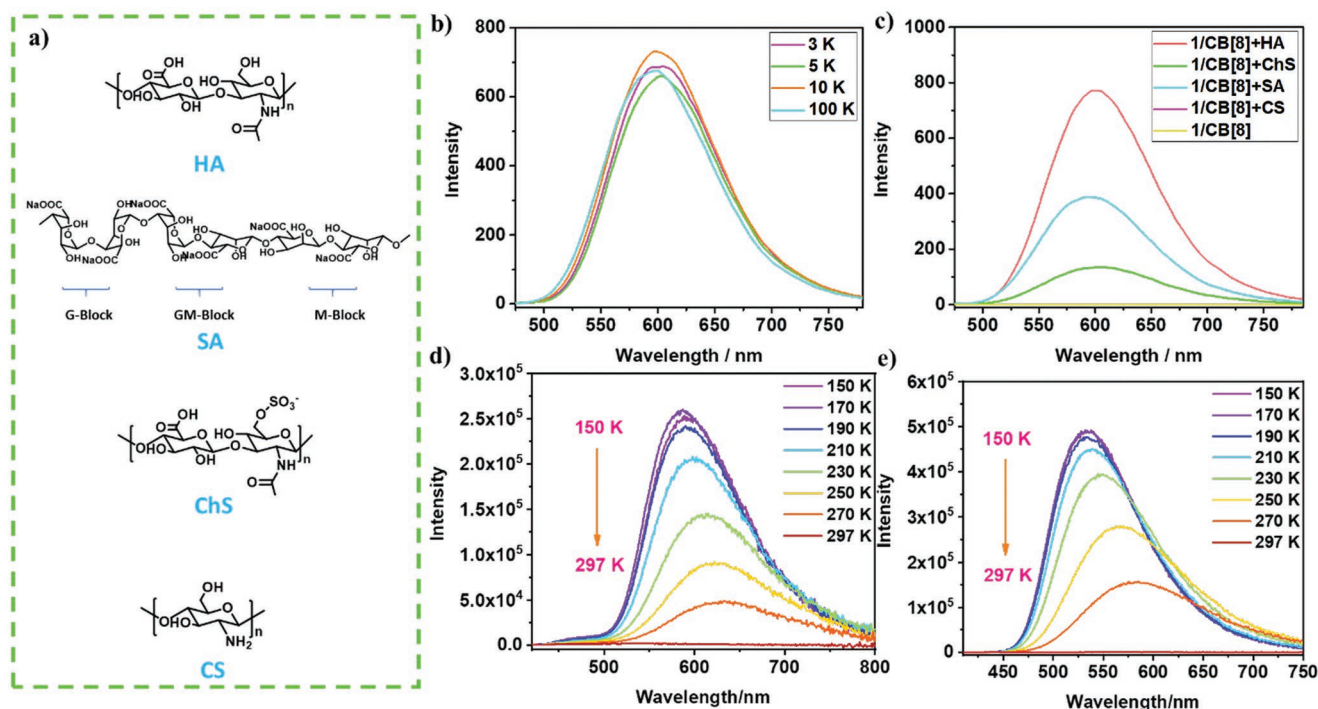


**Figure 5.** a) The chemical structures of various polysaccharide (negatively charged: HA, SA, ChS, and positively charged: CS); b) The fluorescence spectra of 1/CB[8] with adding HA with various molecular weight 3 K (3000), 5 K (5000), 10 K (10 000), and 100 K (100 000); c) The fluorescence spectra of 1/CB[8] with adding various polysaccharide (excitation wavelength: 450 nm, excitation/emission slit: 10/2.5 nm,  $[1] = [CB[8]] = 2 \times 10^{-5} \text{ M}$ ,  $[HA] = 4 \times 10^{-6} \text{ M} = 40 \text{ mg L}^{-1}$ ,  $[ChS] = [SA] = [CS] = 40 \text{ mg L}^{-1}$ ); The fluorescence spectra of d) ( $[1] = 2 \times 10^{-5} \text{ M}$ ), and e) 1' ( $[1'] = 2 \times 10^{-5} \text{ M}$ ) under various temperatures.

positively charged property, which tended to coassemble with negatively charged polysaccharides (Figure S48, Supporting Information). The TEM images proved that the tubular supramolecular polymer 1/CB[8] was divided into smaller nanoparticles and entangled in negatively charged polysaccharides after forming ternary supramolecular systems, suggesting that the host-guest complexes performed secondary reassembly with negatively charged polysaccharides through electrostatic interaction (Figure S49, Supporting Information). The tests of DLS and zeta potential ( $\zeta$ ) showed that the average diameters and  $\zeta$  of ternary supramolecular systems were 83 nm and  $-22.9 \text{ mV}$  for 1/CB[8]+HA, 143 nm and  $-43.1 \text{ mV}$  for 1/CB[8]+SA, 67 nm and  $-25.6 \text{ mV}$  for 1/CB[8]+ChS, respectively (Figures S50 and S51, Supporting Information). Directly mixing 1 or 1' with HA presented large sheet or nanoparticle structures (Figure S52, Supporting Information).

## 2.5. Mechanism Studies

The unique photophysical behavior synergistically unlocked by supramolecular secondary reassembly inspired us to explore the possible mechanism. We speculated that there might be two crucial factors for the efficient fluorescence emission: 1) precisely suppressing the intramolecular rotation of dual-rotor (phenylpyridinium as rotor 1 and anthracene as rotor 2); 2) formation of charge transfer from anthracene to phenylpyridinium. By analyzing the non-emissive properties in aqueous, AIE behavior and structural characteristics of compounds 1 and

1', it could be concluded that the intramolecular rotation played significant roles in the fluorescence emission. Aggregates could effectively inhibit the intramolecular rotation through intermolecular  $\pi$ - $\pi$  stacking, thus promoting the fluorescence emission of compounds 1 and 1' (Figure 2).<sup>[8h]</sup> To further prove this conclusion and dual-rotor characteristic, the cryogenic tests were performed. The intense fluorescence under low temperature and no emission under room temperature for compound 1 manifested that the nonradiative pathway via intramolecular motion was the dominant factor for the photophysical behavior (Figure 5d). After coassembling with CB[8] and HA, the fluorescence emission was enhanced and effectively retained even though rising the temperature from 150 to 297 K (room temperature), hinting the outstanding abilities of CB[8] and HA for suppressing intramolecular motion (Figure S53a, Supporting Information). Moreover, non-emissive behavior from 1/CB[8] and 1+HA under room temperature, which could be awakened by lowering the temperature to 150 K, suggested that individually reducing intramolecular motion of phenylpyridinium through CB[8] or anthracene through HA could not efficiently activate the fluorescence and the nonradiative pathway through rotation was still the dominant factor (Figures S53b,c, Supporting Information). Thus, synergistically restricting rotation of dual-rotor was necessary. Similar phenomenon was also observed for compound 1' and its supramolecular assemblies (Figure 5e and Figure S54, Supporting Information). These results not merely proved that intramolecular rotation was the main channel to exhaust the energy of excited state of anthracene-centered luminogens, but also illustrated that

supramolecular secondary reassembly for synergistically suppressing rotation of dual-rotor was the key for this luminescence performance. On the other hand, the intramolecular charge transfer was the foundation for fluorescence emission at 600 and 570 nm. It was deduced that the large steric hindrance between anthracene and phenylpyridinium caused the twisted molecular conformation and nonconjugated structure of 1 and 1', which could be confirmed by the separated UV-vis absorption bands (Figures S16a,b, Supporting Information). This point was harmful to form twisted intramolecular charge transfer (TICT).<sup>[15]</sup> After complexing with CB[8], the charge transfer was induced with absorption at 450 nm for 1 and 424 nm for 1', both of which were further enhanced through coassembling with HA (Figure S55, Supporting Information). Accordingly, the new fluorescence peaks at 600 nm for 1/CB[8]+HA and 570 nm for 1'/CB[8]+HA with large Stokes shifts occurred (Figure 3a,d). This sufficiently demonstrated the formation of ternary supramolecular assembly and generation of corresponding charge transfer emission. The gradually growing fluorescence intensity was in agreement with the enhanced charge transfer absorption when increasing the concentration of HA, further proving that the emission at 600 nm for 1/CB[8]+HA and 570 nm for 1'/CB[8]+HA originated from charge transfer (Figures S41 and S56, Supporting Information). Expectedly, 1/CB[8] also exhibited the increased charge transfer bands when coassembling with various polysaccharides (ChS and SA) (Figure S57a, Supporting Information). However, there was no similar enhancement for CS, revealing that CS could not coassemble with 1/CB[8] to fabricate ternary supramolecular assembly to inhibit intramolecular rotation of anthracene. The almost unchanged charge transfer absorption explained why the fluorescence behavior of ternary supramolecular assembly was irrelevant to the molecular weight of HA (Figure 5b and Figure S57b, Supporting Information). Intriguingly, the supramolecular assemblies based on CB[7] or directly mixing luminogens (1 or 1') with HA could not induce the charge transfer, corresponding to the non-emissive performance (Figure 5c,f and Figure S58, Supporting Information). Although there was no direct evidence, we deduced that the unique binding mode of CB[8] (two phenylpyridinium in cavity of one CB[8]) played crucial roles in efficiently promoting the formation of TICT and in suppressing the free rotation of phenylpyridinium by intermolecular stacking. The binding constants of molecule 1 and CB[*n*] (*n* = 7, 8) were calculated through the corresponding titration plots of UV-vis spectra (Figure S59, Supporting Information). Molecule 1 showed stronger binding with CB[8] compared to CB[7] and the characterized absorption reached constant when the concentration of CB[8] was above  $4 \times 10^{-5}$  M (two equivalent to molecule 1). For ternary supramolecular assemblies based on CB[7], CB[7] could not form the compact binding with guest molecules similar to CB[8] (Figure S59, Supporting Information). Moreover, the intermolecular stacking structure (two phenylpyridinium in one macrocyclic cavity) to inhibit the intramolecular rotation of phenylpyridinium and to promote formation of charge transfer, existing in CB[8]-based supramolecular systems, was not constructed by CB[7]-based supramolecular systems due to the 1:1 binding mode between CB[7] and phenylpyridinium. Thus, the fluorescence was not activated by CB[7]-based ternary supramolecular systems. Various

macrocyclic compounds, including  $\beta$ -cyclodextrin and its derivatives and pillararene derivative and calixarene derivatives, were used to prove the uniqueness of CB[8]. There was no activated effect similar to CB[8] for these macrocyclic hosts before and after adding HA (Figure S60, Supporting Information). Additionally, the introduction of CB[*n*] (*n* = 7, 8) and HA had no effect on the absorption band of compound 2 (Figure S61, Supporting Information). All of these results jointly proved the significant importance of CB[8] and HA in inducing the fluorescence emission of 1 and 1' through inhibiting intramolecular rotation and promoting formation of intramolecular charge transfer.

## 2.6. Information Encryption and Bioimaging

According to the unique fluorescence cooperatively responding to two compounds and photoresponsive characteristic, these luminescent systems were appropriate use in aspects of information encryption and anti-counterfeiting (Figure 6a and Video S1, Supporting Information). The colorless mixture of 1 in aqueous was used as information source to encrypt the digits of "518." Meanwhile, the other corresponding areas were filled with pure water. No any information could be recognized under daylight and UV light because 1 solution and pure water were colorless and non-emissive even though they were irradiated by 365 nm UV light (Key 3). After spraying the solution of HA (Key 1), all areas of the encryption system were still colorless under daylight. After irradiating with 365 nm portable ultraviolet lamp (Key 3), there was also no observed information because no fluorescence was activated without help of CB[8] due to the fluorescent characteristic responding to two components. Intriguingly, the CB[8] solution as the second key (Key 2) was further introduced to perform decryption, the encrypted system retained unchanged under daylight and the bright orange digits of "518" ultimately appeared and were acquired by us after irradiating the encryption system with 365 nm UV light (Key 3). These results proved that the encrypted message "518" could only be unlocked if the three keys (Key 1, Key 2, and Key 3) were used simultaneously, hinting the extraordinary effect for protecting confidential information. Accordingly, various other encryption systems were also achieved by rational design, including information encryption with polyacrylamide (PAM) hydrogel as matrix (Figures S62–S64, Videos S2 and S3, Supporting Information). Additionally, as a natural polysaccharide widely present in cells and tissues in the human body, HA is universally used in fields of biomedicine and bioimaging.<sup>[16]</sup> Furthermore, HA is able to recognize specific receptors overexpressed on the surface of tumor cells, thus exhibiting huge potential in detection of tumors and therapy of cancer.<sup>[17]</sup> To estimate the bioimaging ability of anthracene-centered emitters in cancer cells, the cell experiments were designed and performed. According to the cytotoxicity test, the ternary supramolecular system 1/CB[8]+HA exhibited low cytotoxicity to normal cells and cancer cells, suggesting that this supramolecular system is biocompatible and probably appropriate as bioimaging reagent for biological applications (Figure S65, Supporting Information). Subsequently, the compound 1 and the corresponding supramolecular systems (1/CB[8], 1+HA,

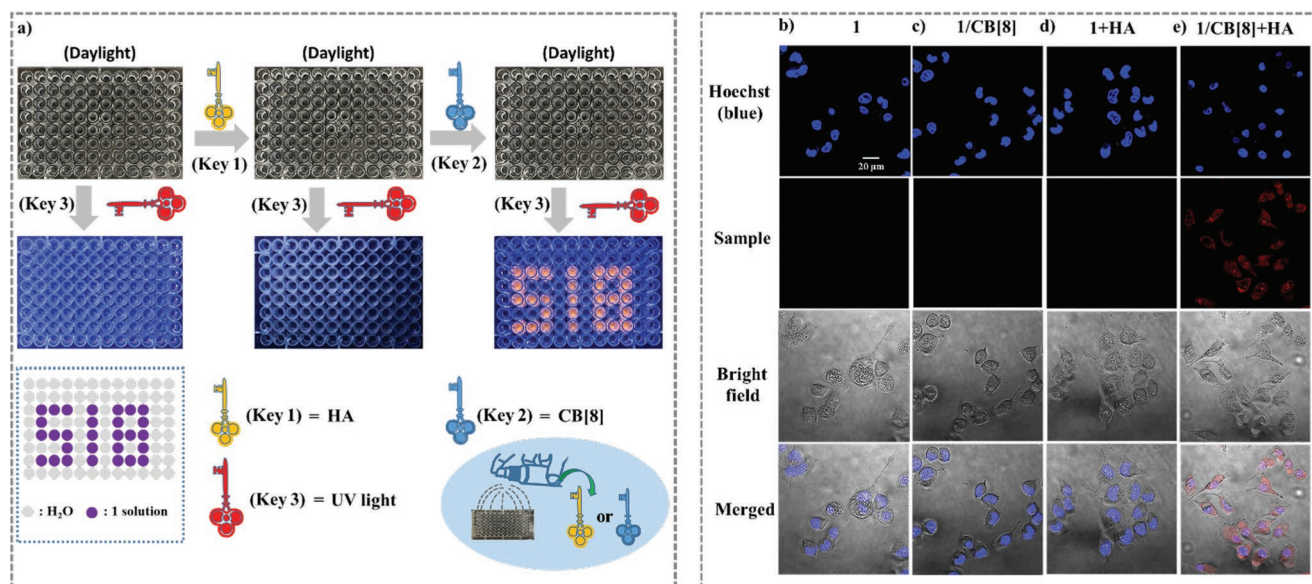


**Figure 6.** a) The triplet encryption information security and decryption constructed by supramolecular secondary reassembly based on 1 and corresponding the supramolecular systems; The confocal fluorescence images of living HeLa cells incubated with b) 1, c) 1/CB[8], d) 1+HA, and e) 1/CB[8]+HA ( $[1] = [\text{CB}[8]] = 5 \times 10^{-6} \text{ M}$ ,  $[\text{HA}] = 10^{-6} \text{ M}$ ).

and 1/CB[8]+HA) were used to incubate with human cervical cancer cells (HeLa cells) for 12 h, respectively. The results presented that the robust red fluorescence was observed through confocal laser scanning microscopy (CLSM) when treating the HeLa cells with ternary supramolecular system 1/CB[8]+HA (Figure 6e). Nevertheless, under the same conditions, there was no signal for HeLa cells treated with compound 1 or 1/CB[8] or 1+HA, manifesting that the robust red fluorescence from ternary supramolecular system was not induced and affected by the intrinsic environment of HeLa cells (Figure 6b–d). Besides, the normal cells 293T cells were selected as a comparison to judge the imaging efficacy of this supramolecular system for normal cells. The intense fluorescence signals for cancer cells (HeLa cells) and weak signals for normal cells (293T cells) demonstrated that this ternary supramolecular system only displayed superior imaging ability for cancer cells (Figure S66, Supporting Information). This was probably attributed to the targeted ability of HA and HA receptors overexpressed on the surface of tumor cells, which gave the ternary supramolecular assembly easier access to the cancer cells and laid an important foundation for realizing targeted tumor detection in vivo.

### 3. Conclusion

In this work, two anthracene-centered emitters (1 and 1') with dual-rotor characteristics are designed to achieve bright fluorescence emission through CB[8] and HA mediated the supramolecular secondary reassembly strategy by precisely suppressing multilevel intramolecular rotation. Due to the various nonradiative pathways from intramolecular rotation of phenylpyridinium (rotor 1) and anthracene (rotor 2), the compounds 1 and 1' display non-emissive characteristic under single molecular state in aqueous. After coassembling with CB[8] and HA, the fluorescence are successfully activated to

generate bright emission with large Stokes shifts (150 nm for 1/CB[8]+HA and 146 nm for 1'/CB[8]+HA) responding to multiple excitation wavelengths. The main factor is supramolecular secondary reassembly, in which CB[8] and HA can effectively suppress the intramolecular rotation of phenylpyridinium and anthracene and promote the intramolecular charge transfer. The quantum yield analysis showed that the fluorescence efficiency from secondary supramolecular assembly (10.01% for 1/CB[8]+HA and 66.83% for 1'/CB[8]+HA) is higher than that of solid state (4.47% for 1 and 9.95% for 1'). In addition, the dual-rotor property endows the fluorescence systems with uniqueness of double lock management. Combing with UV light as the third key, we successfully achieve the triple encryption information security. Furthermore, the participation of HA makes the supramolecular luminescent systems show huge potential in application of bioimaging and cancer treatment. Therefore, this work not only provides novelty dual-rotor luminescence through precisely inhibiting multilevel intramolecular motion, but also offers a possible reference to design multiple components stimuli-responsive smart luminescent materials and targeted bioimaging.

### Supporting Information

Supporting Information is available from the Wiley Online Library or from the author.

### Acknowledgements

The authors thank the Haihe Laboratory of Sustainable Chemical Transformations for the financial support. This work was financially supported by the National Natural Science Foundation of China (Grant No. 22131008) and the Fundamental Research Funds for the Central Universities, Nankai University.

## Conflict of Interest

The authors declare no conflict of interest.

## Author Contributions

W.-W.X. and Y.-X.Q. contributed equally to this work. Y.L. and W.-W.X. conceived the idea and designed the research. W.-W.X. and Y.-X.Q. performed the experiment. J.N., Y.-X.Q. and W.X. finished the cell experiments and information encryption experiments. Y.L. and W.-W.X. wrote the manuscript of this work. Y.C. and H.-Y.Z. provided constructive suggestions for results and helped revise the paper. All authors participated in the discussion.

## Data Availability Statement

The data that support the findings of this study are available from the corresponding author upon reasonable request.

## Keywords

aggregation-induced emission, cucurbiturils, dual-rotor, hyaluronic acid, information encryption, supramolecular reassembly

Received: October 15, 2022

Revised: November 8, 2022

Published online: December 8, 2022

- [1] a) G. Feng, B. Liu, *Acc. Chem. Res.* **2018**, *51*, 1404; b) A. Kaur, E. J. New, *Acc. Chem. Res.* **2019**, *52*, 623; c) H. M. Kim, B. R. Cho, *Chem. Rev.* **2015**, *115*, 5014; d) S. K. Behera, S. Y. Park, J. Gierschner, *Angew. Chem., Int. Ed.* **2021**, *60*, 22624.
- [2] a) T. L. Mako, J. M. Racicot, M. Levine, *Chem. Rev.* **2019**, *119*, 322; b) K. Y. Zhang, Q. Yu, H. Wei, S. Liu, Q. Zhao, W. Huang, *Chem. Rev.* **2018**, *118*, 1770.
- [3] a) X. Huang, J. Song, B. C. Yung, X. Huang, Y. Xiong, X. Chen, *Chem. Soc. Rev.* **2018**, *47*, 2873; b) M. H. Lee, J. S. Kim, J. L. Sessler, *Chem. Soc. Rev.* **2015**, *44*, 4185.
- [4] a) Y. Liu, C. Li, Z. Ren, S. Yan, M. R. Bryce, *Nat. Rev. Mater.* **2018**, *3*, 18020; b) M. Y. Wong, E. Zysman-Colman, *Adv. Mater.* **2017**, *29*, 1605444.
- [5] a) A. Abdollahi, H. Roghani-Mamaqani, B. Razavi, M. Salami-Kalajahi, *ACS Nano* **2020**, *14*, 14417; b) W. Ren, G. Lin, C. Clarke, J. Zhou, D. Jin, *Adv. Mater.* **2020**, *32*, 1901430.
- [6] a) W. Zhao, Z. He, B. Z. Tang, *Nat. Rev. Mater.* **2020**, *5*, 869; b) C. W. Zhu, K. Shoyama, F. Wurthner, *Angew. Chem., Int. Ed.* **2020**, *59*, 21505.
- [7] a) N. Aizawa, A. Matsumoto, T. Yasuda, *Sci. Adv.* **2021**, *7*, 5769; b) D. Cao, Z. Liu, P. Verwilst, S. Koo, P. Jangjili, J. S. Kim, W. Lin, *Chem. Rev.* **2019**, *119*, 10403; c) X.-K. Chen, D. Kim, J.-L. Brédas, *Acc. Chem. Res.* **2018**, *51*, 2215; d) L. Huang, L. Liu, X. Li, H. Hu, M. Chen, Q. Yang, Z. Ma, X. Jia, *Angew. Chem., Int. Ed.* **2019**, *58*, 16445; e) A. Khan, X. Tang, C. Zhong, Q. Wang, S.-Y. Yang, F.-C. Kong, S. Yuan, A. S. D. Sandanayaka, C. Adachi, Z.-Q. Jiang, L.-S. Liao, *Adv. Funct. Mater.* **2021**, *31*, 2009488; f) X. Li, Z. Li, Y.-W. Yang, *Adv. Mater.* **2018**, *30*, 1800177; g) W. Ma, Y. Su, Q. Zhang, C. Deng, L. Pasquali, W. Zhu, Y. Tian, P. Ran, Z. Chen, G. Yang, G. Liang, T. Liu, H. Zhu, P. Huang, H. Zhong, K. Wang, S. Peng, J. Xia, H. Liu, X. Liu, Y. M. Yang, *Nat. Mater.* **2022**, *21*, 210; h) J. Qi, J. Li, R. Liu, Q. Li, H. Zhang, J. W. Y. Lam, R. T. K. Kwok, D. Liu, D. Ding, B. Z. Tang, *Chem* **2019**, *5*, 2657; i) Z.-B. Sun, J.-K. Liu, D.-F. Yuan, Z.-H. Zhao, X.-Z. Zhu, D.-H. Liu, Q. Peng, C.-H. Zhao, *Angew. Chem., Int. Ed.* **2019**, *58*, 4840; j) C. Wang, S. R. Adams, E. T. Ahrens, *Acc. Chem. Res.* **2021**, *54*, 3060; k) R. Yang, X. Ren, L. Mei, G. Pan, X.-Z. Li, Z. Wu, S. Zhang, W. Ma, W. Yu, H.-H. Fang, C. Li, M.-Q. Zhu, Z. Hu, T. Sun, B. Xu, W. Tian, *Angew. Chem., Int. Ed.* **2022**, *134*, e202117158.
- [8] a) X.-M. Chen, X.-F. Hou, H. K. Bisoyi, W.-J. Feng, Q. Cao, S. Huang, H. Yang, D. Chen, Q. Li, *Nat. Commun.* **2021**, *12*, 4993; b) X. Li, Y. Xie, B. Song, H.-L. Zhang, H. Chen, H. Cai, W. Liu, Y. Tang, *Angew. Chem., Int. Ed.* **2017**, *56*, 2689; c) G. Perli, Q. Wang, C. B. Braga, D. L. Bertuzzi, L. A. Fontana, M. C. P. Soares, J. Ruiz, J. D. Megiatto, D. Astruc, C. Ornelas, *J. Am. Chem. Soc.* **2021**, *143*, 12948; d) N. Song, Z. Zhang, P. Liu, Y.-W. Yang, L. Wang, D. Wang, B. Z. Tang, *Adv. Mater.* **2020**, *32*, 2004208; e) R. Tian, Q. Zeng, S. Zhu, J. Lau, S. Chandra, R. Ertsey, K. S. Hettie, T. Teraphongphom, Z. Hu, G. Niu, D. O. Kiesewetter, H. Sun, X. Zhang, A. L. Antaris, B. R. Brooks, X. Chen, *Sci. Adv.* **2019**, *5*, 0672; f) X. Ma, J. Wang, H. Tian, *Acc. Chem. Res.* **2019**, *52*, 738; g) R. Wang, K.-H. Kim, J. Yoo, X. Li, N. Kwon, Y.-H. Jeon, S.-k. Shin, S. S. Han, D.-S. Lee, J. Yoon, ACS Nano **2022**, *16*, 3045; h) Q. Zeng, Z. Li, Y. Dong, C. A. Di, A. Qin, Y. Hong, L. Ji, Z. Zhu, C. K. W. Jim, G. Yu, Q. Li, Z. Li, Y. Liu, J. Qin, B. Z. Tang, *Chem. Commun.* **2007**, 70.
- [9] a) L. Hu, K. Li, W. Shang, X. Zhu, M. Liu, *Angew. Chem., Int. Ed.* **2020**, *59*, 4953; b) L. Hu, X. Zhu, C. Yang, M. Liu, *Angew. Chem., Int. Ed.* **2022**, *61*, e202114759; c) P. Xiao, C. Liu, T. Ma, X. Lu, L. Jing, Y. Hou, P. Zhang, G. Huang, M. Gao, *Adv. Sci.* **2021**, *8*, 2004044; d) Q.-W. Zhang, D. Li, X. Li, P. B. White, J. Mecninović, X. Ma, H. Ågren, R. J. M. Nolte, H. Tian, *J. Am. Chem. Soc.* **2016**, *138*, 13541; e) Y. Sun, Y. Chen, L. Jiang, X. Yu, Y. Qin, S. Wang, Y. Liu, *Adv. Opt. Mater.* **2022**, *10*, 2201330.
- [10] a) F.-F. Shen, Y. Chen, X. Xu, H.-J. Yu, H. Wang, Y. Liu, *Small* **2021**, *17*, 2101185; b) H. Wu, Y. Chen, X. Dai, P. Li, J. F. Stoddart, Y. Liu, *J. Am. Chem. Soc.* **2019**, *141*, 6583; c) G. Wu, Z. Huang, O. A. Scherman, *Angew. Chem., Int. Ed.* **2020**, *59*, 15963; d) G. Wu, Y. J. Bae, M. Olesińska, D. Antón-García, I. Szabó, E. Rosta, M. R. Wasielewski, O. A. Scherman, *Chem. Sci.* **2020**, *11*, 812.
- [11] a) A. H. G. David, R. Casares, J. M. Cuerva, A. G. Campaña, V. Blanco, *J. Am. Chem. Soc.* **2019**, *141*, 18064; b) H. Wu, Y. Chen, Y. Liu, *Adv. Mater.* **2017**, *29*, 1605271; c) Y. Zhou, H.-Y. Zhang, Z.-Y. Zhang, Y. Liu, *J. Am. Chem. Soc.* **2017**, *139*, 7168; d) H. Wang, W. Xing, Z. Yu, H. Zhang, W. Xu, Y. Liu, *Adv. Opt. Mater.* **2022**, <https://doi.org/10.1002/adom.202201903>.
- [12] a) S. Guo, Y. Song, Y. He, X.-Y. Hu, L. Wang, *Angew. Chem., Int. Ed.* **2018**, *57*, 3163; b) J. H. Lee, S. H. Jung, S. S. Lee, K.-Y. Kwon, K. Sakurai, J. Jaworski, J. H. Jung, *ACS Nano* **2017**, *11*, 4155; c) M. A. H. Muhammed, L. K. Cruz, A.-H. Emwas, A. M. El-Zohry, B. Moosa, O. F. Mohammed, N. M. Khashab, *Angew. Chem., Int. Ed.* **2019**, *58*, 15665; d) Y. Sun, F. Guo, T. Zuo, J. Hua, G. Diao, *Nat. Commun.* **2016**, *7*, 12042.
- [13] a) J. Du, L. Sheng, Y. Xu, Q. Chen, C. Gu, M. Li, S. X.-A. Zhang, *Adv. Mater.* **2021**, *33*, 2008055; b) J. Gao, M. Tian, Y. He, H. Yi, J. Guo, *Adv. Funct. Mater.* **2022**, *32*, 2107145; c) Y. Hou, Z. Zhang, S. Lu, J. Yuan, Q. Zhu, W.-P. Chen, S. Ling, X. Li, Y.-Z. Zheng, K. Zhu, M. Zhang, *J. Am. Chem. Soc.* **2020**, *142*, 18763; d) C. Shu, L. Fang, M. Yang, L. Zhong, X. Chen, D. Yu, *Angew. Chem., Int. Ed.* **2022**, *61*, e202114182; e) M. Tu, H. Reinsch, S. Rodríguez-Hermida, R. Verbeke, T. Stassin, W. Egger, M. Dickmann, B. Dieu, J. Hofkens, I. F. J. Vankelecom, N. Stock, R. Ameloot, *Angew. Chem., Int. Ed.* **2019**, *58*, 2423; f) F. Bian, L. Sun, H. Chen, Y. Wang, L. Wang, L. Shang, Y. Zhao, *Adv. Sci.* **2022**, *9*, 2105278; g) H. Kishimoto, M. Zhao, K. Hayashi, Y. Urata, N. Tanaka, T. Fujiwara, S. Penman, R. M. Hoffman, *Proc. Natl. Acad. Sci. USA* **2009**, *106*, 14514; h) J. Dai,

- H. Xue, D. Chen, X. Lou, F. Xia, S. Wang, *Coord. Chem. Rev.* **2022**, 464, 214552; i) R. W. Gao, N. T. Teraphongphom, N. S. van den Berg, B. A. Martin, N. J. Oberhelman, V. Divi, M. J. Kaplan, S. S. Hong, G. Lu, R. Ertsey, W. S. F. J. Tummers, A. J. Gomez, F. C. Holsinger, C. S. Kong, A. D. Colevas, J. M. Warram, E. L. Rosenthal, *Cancer Res.* **2018**, 78, 5144; j) M. Ling, R. Sun, G. Li, M. Z. Syeda, W. Ma, Z. Mai, L. Shao, L. Tang, Z. Yu, *Nano Res.* **2022**, 15, 6288.
- [14] a) W.-W. Xu, Y. Chen, Y.-L. Lu, Y.-X. Qin, H. Zhang, X. Xu, Y. Liu, *Angew. Chem., Int. Ed.* **2022**, 61, e202115265; b) Z.-Y. Zhang, W.-W. Xu, W.-S. Xu, J. Niu, X.-H. Sun, Y. Liu, *Angew. Chem., Int. Ed.* **2020**, 59, 18748.
- [15] S. Sasaki, G. P. C. Drummen, G.-i. Konishi, *J. Mater. Chem. C* **2016**, 4, 2731.
- [16] J. A. Burdick, G. D. Prestwich, *Adv. Mater.* **2011**, 23, H41.
- [17] G. Huang, H. Huang, *Drug Delivery* **2018**, 25, 766.